Materials Science & Engineering A 748 (2019) 228–235

Contents lists available at ScienceDirect

Materials Science & Engineering A

journal homepage: www.elsevier.com/locate/msea

Effect of second phase particles on mechanical properties and grain growth in a CoCrFeMnNi high entropy alloy

M.V. Klimova*, D.G. Shaysultanov, S.V. Zherebtsov, N.D. Stepanov

Laboratory of Bulk Nanostructured Materials, Belgorod National Research University, Pobeda 85, Belgorod 308015, Russia

ARTICLE INFO

Keywords:
High entropy alloys
Phase transformations
Grains and interfaces
Electron microscopy
Stress/strain measurements

ABSTRACT

Effect of annealing of a cold-worked CoCrFeMnNi alloy at temperatures of 500–900 °C for 1–50 h on the structure and mechanical properties was studied in the present work. Annealing for an hour resulted in: i) recrystallization of the face-centered cubic (fcc) matrix at 600–900 °C; ii) precipitation of a Cr-rich body-centered cubic (bcc) phase at 500–700 °C or a sigma phase particles at 600–800 °C. Moreover, an increase in the annealing time to 50 h at 600 °C resulted in a continuous growth of both the fcc grans and bcc/sigma particles and in an increase in the fraction of the sigma phase at the expense of the bcc phase particles. The fcc grains growth was found to be controlled by the pinning effect of the second phase particles. Soaking for an hour at 500–600 °C resulted in a substantial increase in strength of the alloy due to the second phases precipitation. Meanwhile annealing at the higher temperatures as well as an increase in the annealing time at 600 °C resulted in softening; however, even after 50 h annealing, the alloy demonstrated reasonably high strength. In the latter case fine fcc grains, preserved due to the pinning effect by the second phases particles, contributed to strength mainly.

1. Introduction

The so-called high-entropy alloys have recently emerged as a new class of advanced metallic materials with complex, multicomponent chemical composition. It is believed that among the extreme vastness of possible compositions and structures some of these alloys can possess unique properties [1]. Some of the promising HEAs are those which base on 3d transition elements and have a face-centered cubic (fcc) structure [2]; a representative of this class is the equiatomic CoCrFeMnNi alloy [2,3]. It has a single fcc random solid solution phase structure which is stable at high temperatures (≥900 °C) [4–8]. The alloy has also very high ductility and fracture toughness at room and cryogenic temperatures, making it promising for cryogenic applications [9–11]. The yield strength of the alloy at room temperature is rather low, however. Precipitation strengthening due to alloying by additional elements, such as Al, Ti, C, etc., was found to be particularly effective [12–20].

Meanwhile, it is well established that the "pure" CoCrFeMnNi alloy is also prone to the second phases precipitating after heat treatments (annealing) at temperatures below 900 °C [4–8]. These precipitations included sigma, body-centered cubic (bcc), $L1_0$, and B2 phases depending on the exact conditions (i.e. time and temperature of the annealing treatment). It was shown earlier with respect to other HEAs that, for example, the sigma phase can be effectively utilized for strengthening [21,22]. However, only a few studies have examined the influence of the second phase precipitations on the mechanical behavior of the CoCrFeMnNi alloy [6,23].

The second phase(s) particles can also affect various processes in the fcc matrix, for example grain growth. It was recently demonstrated that in CoCrFeNi(Mn, Al, C) alloys second phases precipitations (mostly B2 phase particles) can effectively impede grain growth and can result in the formation of a fine-grained microstructure [24–26]. Alloys with the fine-grained recrystallized microstructure can have an attractive combination of strength, ductility, and fatigue resistance. Meanwhile, it is unclear if the same approach can work in the "pure" CoCrFeMnNi alloy. Moreover, the understanding of both grain growth and particle coarsening in HEAs is lacking at the moment [13,20,25,27–30], despite the fact that both of these processes are crucial for the production of alloys with desirable microstructures and properties.

Therefore, in the present work, we have performed a detailed investigation of structure and mechanical properties of the CoCrFeMnNi high-entropy alloy after cold rolling and subsequent annealing at 500–900 °C for 1–50 h. The aim of the investigation was (i) to gain insight into the kinetics of both grain growth and second phases coarsening in the alloy as well as to establish their interdependence; (ii) to estimate the effect of the second phases precipitation on mechanical

* Corresponding author.
E-mail address: klimova_mv@bsu.edu.ru (M.V. Klimova).

https://doi.org/10.1016/j.msea.2019.01.112
Received 29 November 2018; Received in revised form 28 January 2019; Accepted 30 January 2019
Available online 31 January 2019
0921-5093/

properties of the alloy.

2. Materials and methods

The equiatomic CoCrFeMnNi alloy ($Co_{20.6}Cr_{19.9}Fe_{19.5}Ni_{20.9}Mn_{19.1}$ in at%) was produced by vacuum arc melting and homogenized at 1000 °C for 24 h. The homogenized alloy was cold-rolled to 80% reduction and then annealed at 500 °C, 600 °C, 700 °C, 800 °C or 900 °C for 1 h, and for 1, 2, 5 10 or 50 h at 600 °C; the annealing was followed by air cooling. Additional details of the alloy production and processing can also be found elsewhere [6,21].

The microstructure of the alloy was studied by scanning (SEM) and transmission (TEM) electron microscopy. Samples for SEM observations were prepared by careful mechanical polishing. SEM studies were performed using FEI Quanta 600 FEG microscope equipped with a backscattered electron (BSE) detector. Samples for TEM analysis were prepared by conventional twin-jet electro-polishing of mechanically pre-thinned to 100 μm foils, using an electrolyte composed of 95% C_2H_5OH and 5% $HClO_4$ at a voltage of 27 V at room temperature. TEM investigations were performed using a JEOL JEM-2100 apparatus equipped with an X-ray energy dispersive spectrometry (EDS) detector at an accelerating voltage of 200 kV. Selected area electron diffraction (SAEDs) patterns were used for the phase identification and EDS analysis – for chemical analysis. The size/fractions of recrystallized grains and size/number of precipitates were quantified using at least 10 SEM (for grains and coarse particles) or TEM (for nanoparticles) images with low magnification. For each structural constituent in particular condition, more than 10^3 individual measurements were made to obtain representative statistics. For a careful calculation of the effects of precipitates on the recrystallization behavior, the parameters of particles of different types were determined separately; e.g. sigma particles were distinguished from the bcc ones; the particles located inside the fcc grains and at grain boundaries were also evaluated separately.

Specimens with the gauge dimensions of $6 \times 3 \times 1\ mm^3$ were used for mechanical tests which consisted in tension at a constant crosshead speed of $10^{-3}\ s^{-1}$ to fracture. The long axis of the specimens was aligned with the rolling direction. Elongation to fracture was determined by the measurements of spacing between marks designating the gauge length (before and after the test). At least two samples in each condition were tested. The microhardness of the specimens was examined using Vickers microhardness testing with a load of 0.2 kg. The hardness values were averaged over at least 20 individual measurements for each data point.

3. Results

3.1. Microstructure

3.1.1. Initial microstructure

Microstructure of the CoCrFeMnNi alloy in the cold-rolled condition (80% reduction) is presented in Fig. 1. The cold-rolled alloy had a single-phase heavily-deformed lamellar microstructure composed of twin boundaries and shear bands mostly aligned with the rolling direction. The grains/subgrains transverse size was of about 70 nm. (Fig. 1, see also [31]).

3.1.2. Effect of isochronal annealing

Fig. 2 illustrates the effect of annealing of the cold-rolled CoCrFeMnNi alloy at a temperature in the range of 500–900 °C for 1 h. Annealing at the lowest temperature (500 °C) did not result in significant changes of microstructure in comparison to that of deformed condition; yet some bcc phase particles appeared in the fcc matrix (Fig. 2a, Table 1).

At a higher temperature (600 °C) the majority of the fcc matrix was found to be recrystallized with a size of the recrystallized grains of 1.3 μm (Fig. 2b). The fraction of unrecrystallized areas was 0.35

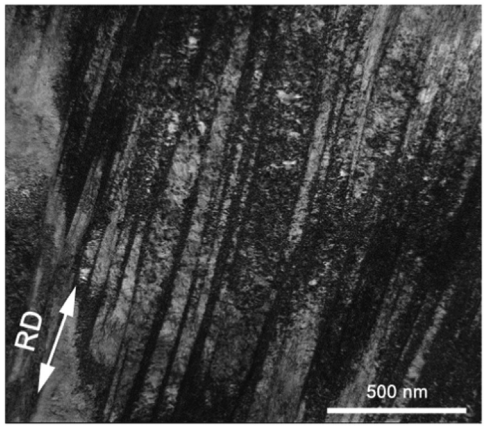

Fig. 1. TEM bright-field image of the structure of the CoCrFeMnNi alloy after 80% cold rolling.

(Table 1). In addition sigma phase particles were observed in the microstructure; sigma particles were coarser and had a rectangular shape, while the bcc particles were found to be round and very fine (Table 1). The bcc particles were distributed homogeneously; the sigma phase particles were located predominantly at the boundaries. However, some sigma particles were also found inside the fcc matrix grains. Particles of both types (bcc and sigma) were mostly composed of Cr (Table 2).

Further increase in annealing temperature resulted in complete recrystallization and led to a gradual increase in the fcc grain size from 2.0 μm after annealing at 700 °C to 17.1 μm – at 900 °C (Fig. 2c-e, Table 1). The alloy contained both the bcc and sigma particles after annealing at 700 °C; yet the fraction of the bcc phase particles was significantly lower than that of the sigma phase. Only a small amount of the sigma particles was found at some grain boundaries after annealing at 800 °C, and no particles were detected after annealing at 900 °C. Note the presence of multiple annealing twins in fcc grains.

3.1.3. Isothermal annealing at 600 °C

Typical microstructures formed in the cold rolled alloy after annealing at 600 °C for 2–50 h are shown in Fig. 3. Annealing was accompanied by a pronounced increase in the recrystallized fraction; already after 5 h of annealing the recrystallized volume comprised 0.95 of a sample. At the same time recrystallized grains growth occurred; the average grain size increased from 1.3 μm to 3.8 μm with an increase in the annealing time from 1 to 50 h (Table 3). A number of near-equilibrium triple junctions of grain boundaries and annealing twins observed in Fig. 3 suggest normal grain growth as the main mechanism of microstructure evolution.

The grain growth occurred concurrently with the second phases particles coarsening (Fig. 3, Table 3), however different types of particles coarsened to a different extent. For instance, the sigma particles located at grain boundaries increased from 260 to 820 nm with an increase in the annealing time from 1 to 50 h; the bcc particles under the same conditions increased from 70 to 120 nm only. At the same time the fraction of the bcc particles decreased from 1.2% to 0.37% (for 1–50 h annealing) while the sigma phase particles fraction increased from 2.0% to 7.4% after 1 and 50 h of annealing, respectively.

A power law function of annealing time (t) is commonly used to calculate the grain/particle size $d \sim t^{1/n}$ [32]. The kinetics of both fcc grain growth and particles coarsening during annealing at 600 °C is shown in Fig. 4 in a log-log scale. It is clearly seen that the size of grains, sigma particles, and bcc particles can be related to the annealing time with the growth exponent n of about 3.6, 4, and 7 respectively.

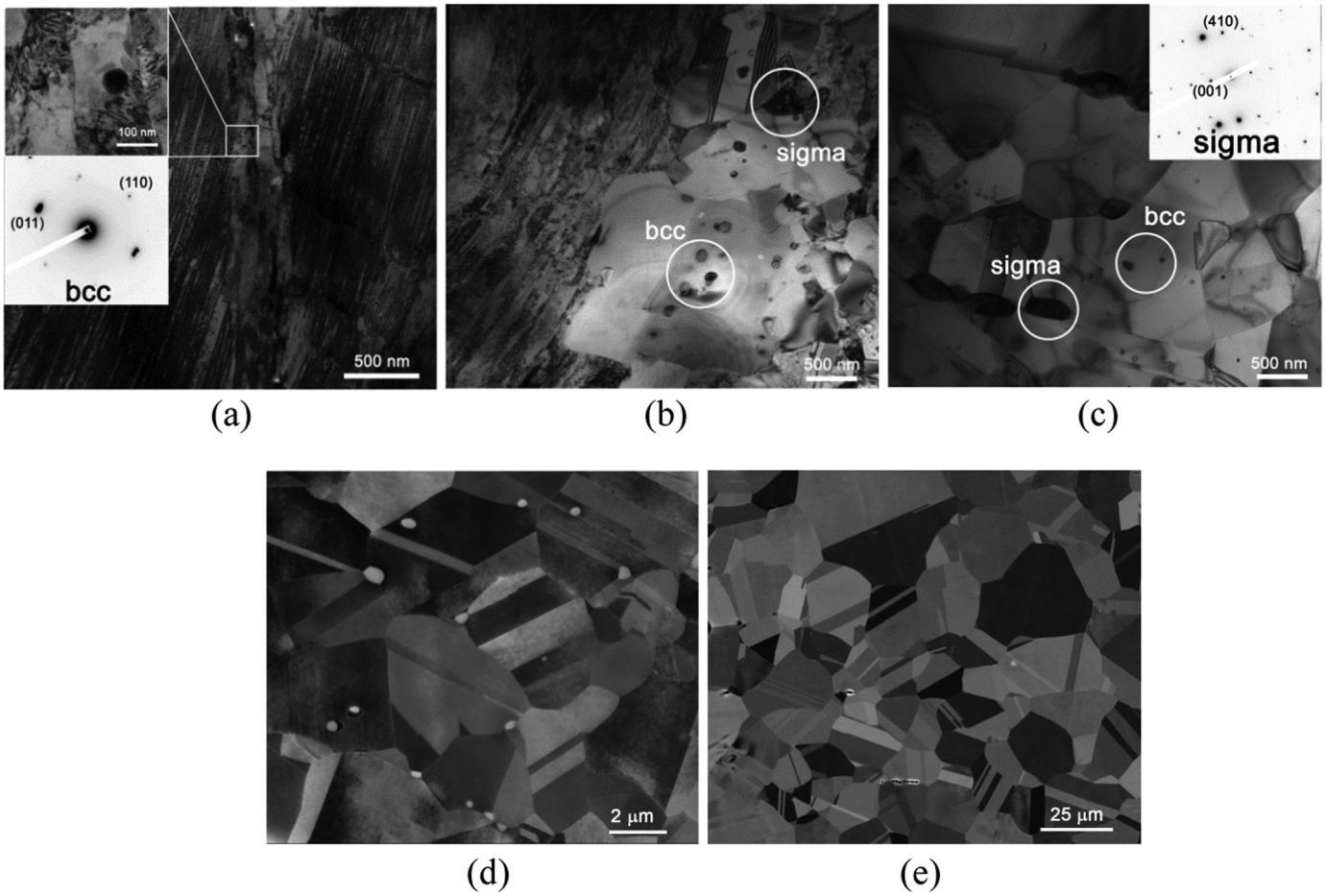

Fig. 2. Structure of the CoCrFeMnNi alloy after annealing for 1 h at: (a) - 500 °C; (b) - 600 °C; (c) - 700 °C; (d) - 800 °C; (e) - 900 °C; (a-c) are TEM bright-field images, (d, e) – SEM-BSE images. Representative SAEDs are given in (a) and (c).

3.2. Mechanical properties

3.2.1. Effect of isochronal annealing

Fig. 5 displays the stress-strain curves of the CoCrFeMnNi alloy in different conditions. The resulting mechanical properties, namely yield strength (YS), ultimate tensile strength (UTS), uniform elongation (UE), and elongation to fracture (EF) are summarized in Table 4. In the cold-rolled condition, the alloy exhibited high strength (YS = 1120 MPa), but relatively low ductility (EF = 14%). Surprisingly, annealing at 500 or 600 °C has resulted in quite a pronounced increase in strength (YS = 1290 MPa and 1155 MPa, respectively) together with a reduction in ductility (EF = 3.6% and 6.7%, respectively). Annealing at higher temperatures in the range of 700–900 °C resulted in a decrease in strength (YS = 270–585 MPa) and a pronounced increase in ductility (EF = 43–60%).

3.2.2. Effect of isothermal annealing

Microhardness measurements were used to estimate the effect of annealing duration at 600 °C on strength of the CoCrFeMnNi alloys (Fig. 6). The cold-rolled alloy had a high hardness of 374 HV. Similarly to the tensile strength (Table 4), a short-time annealing (1–2 h) resulted in somewhat higher hardness of 386–393 HV. However, the alloy softened considerably with an increase in the annealing time attaining 276 HV after annealing for 50 h.

To gain more insight into the effect of annealing time on mechanical behavior of the alloy, tensile testing of the specimen after 1 and 50 h annealing was performed (Fig. 7). As it was shown earlier (Fig. 5,

Table 2
Chemical composition of the constitutive phases in the CoCrFeMnNi alloy after 1-h annealing at 700 °C.

Elements	Co	Cr	Fe	Mn	Ni
Fcc matrix	20.8	18.5	19.8	21.0	19.9
Bcc particles	17.3	36.5	18.0	16.1	12.1
Sigma particles	16.2	43.8	17.6	14.6	7.8

Table 1
Structure parameters of the CoCrFeMnNi alloy after 1-h annealing at different temperatures.

Annealing temperature, °C		500	600	700	800	900
Bcc particles	Fraction, %	0.8 ± 0.05	1.2 ± 0.20	0.4 ± 0.02	–	–
	Size, nm	35 ± 15	70 ± 16	75 ± 15	–	–
Sigma particles	Fraction, %	–	2.1 ± 0.5	2.7 ± 0.6	0.2 ± 0.01	–
	Size, nm	–	220 ± 115	310 ± 130	420 ± 135	–
Recrystallized fcc grains	Fraction, %	–	65 ± 15	100	100	100
	Size, μm	–	1.3 ± 0.7	2.0 ± 0.9	3.6 ± 1.7	17.1 ± 8.2

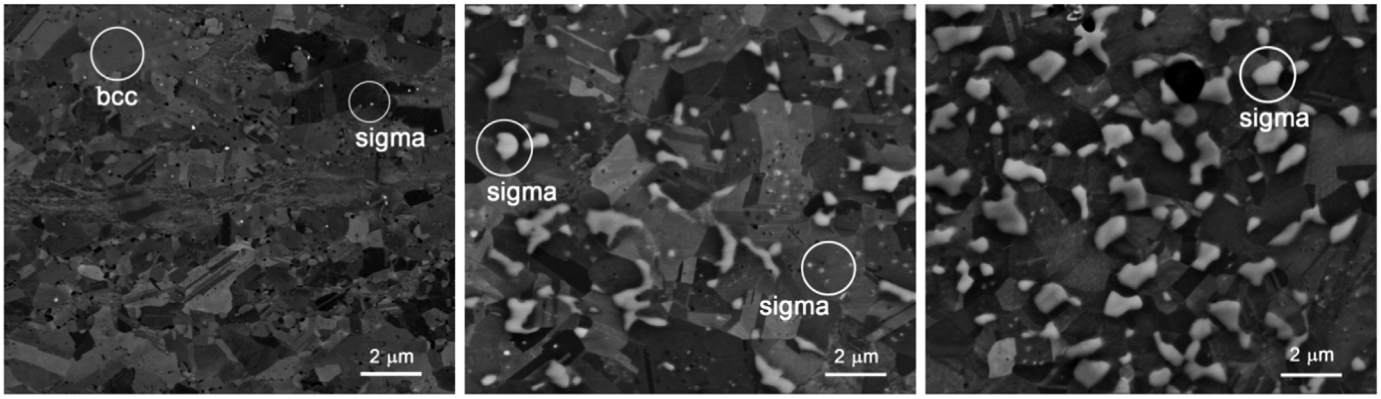

Fig. 3. Structure of the CoCrFeMnNi alloy after annealing at 600 °C for: (a) – 2 h; (b) – 10 h; (c) – 50 h.

Table 4), after 1-h annealing the alloy had high strength but rather low ductility. An increase in the annealing time has resulted in softening and increase of ductility. However, the strength of the alloy was retained on a rather high level: YS = 685 MPa and UTS = 880 MPa. Despite rather weak strain hardening (Fig. 6) the alloy also demonstrated modest UE of 14%.

4. Discussion

4.1. Microstructural response

The obtained results shows that the annealing at 500–900 °C for 1 h of the cold worked CoCrFeMnNi alloy resulted in (i) recrystallization of the fcc matrix (at 600–900 °C) and (ii) precipitation of the Cr-rich bcc (at 500–700 °C) and sigma (at 600–800 °C) particles (Fig. 2, Table 1). The development of recrystallization at T ≥ 600 °C in this alloy was reported earlier several times [7,27–29,33,34]; therefore an increase in both size and fraction of recrystallized grains with increasing temperature is anticipated. The assortment of the observed second phases and the sequence of their precipitation (i.e. bcc at 500–700 °C and sigma at 600–800 °C) were also in agreement with previous reports [4,6,7]. The complex dependence of the fractions and sizes of the constitutive phases on the annealing temperature were most likely caused by an intricate relation between the kinetics (diffusion activity increases with temperature) and thermodynamic (equilibrium fraction of the second phase particles usually decreases with temperature) factors.

Meanwhile an increase in the annealing duration at 600 °C from 1 to 50 h led to less expected results in terms of the alloy phase composition. Namely, the fraction of the bcc phase particles decreased pronouncedly, while the sigma phase fraction increased (Table 3). It should be noted, however, that as per the CALPHAD calculation results [35,36], the sigma phase is the only equilibrium phase in the alloy at 600 °C except for the fcc matrix. At the same time the sigma phase has a complex tetragonal crystal structure which retards the precipitation kinetics [37,38]. On the other side the disordered bcc phase (also enriched with Cr) can be a metastable intermediate phase which appeared at the

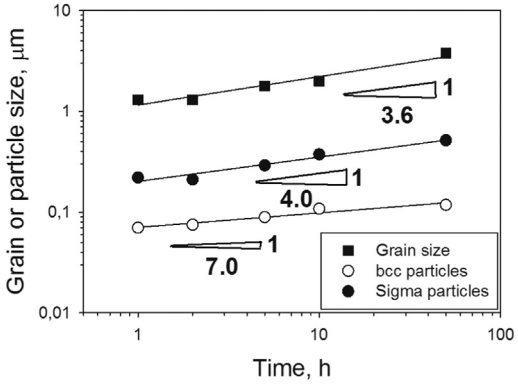

Fig. 4. Size of the fcc grains and bcc or sigma particles as a function of annealing time at 600 °C.

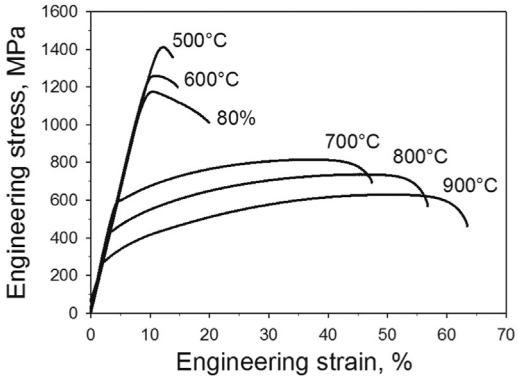

Fig. 5. Engineering stress-strain curves of the CoCrFeMnNi alloy after 80% cold rolling and subsequent annealing at 500–900 °C.

Table 3
Structure parameters of the CoCrFeMnNi alloy after annealing at 600 °C for 1–50 h.

Annealing time, h		1	2	5	10	50
Bcc particles	Fraction, %	1.2 ± 0.20	1.0 ± 0.13	0.73 ± 0.11	0.54 ± 0.07	0.37 ± 0.03
	Size, nm	70 ± 16	76 ± 23	89 ± 31	108 ± 41	118 ± 47
Sigma particles	Fraction, %	2.0 ± 0.5	2.6 ± 0.8	3.9 ± 1.4	5.4 ± 2.1	7.4 ± 1.9
	Size, nm	220 ± 115	211 ± 132	292 ± 180	374 ± 250	515 ± 380
Recrystallized fcc grains	Fraction, %	65 ± 15	72 ± 5	95 ± 5	100	100
	Size, μm	1.3 ± 0.7	1.3 ± 0.4	1.8 ± 0.6	2.0 ± 0.8	3.8 ± 1.9

Table 4
Mechanical properties of the CoCrFeMnNi alloy after 80% cold rolling and subsequent annealing at 500–900 °C: yield strength (YS), ultimate tensile strength (UTS), uniform elongation (UE), and elongation to fracture (EF).

Condition	YS, MPa	UTS, MPa	UE, %	EF, %
80% rolling	1120	1175	1.5	14.0
80% rolling + annealing 500 °C	1290	1415	1.1	3.6
80% rolling + annealing 600 °C	1135	1260	1.8	6.7
80% rolling + annealing 700 °C	585	815	31.7	42.7
80% rolling + annealing 800 °C	425	735	40.2	52.5
80% rolling + annealing 900 °C	270	630	46.2	60.5

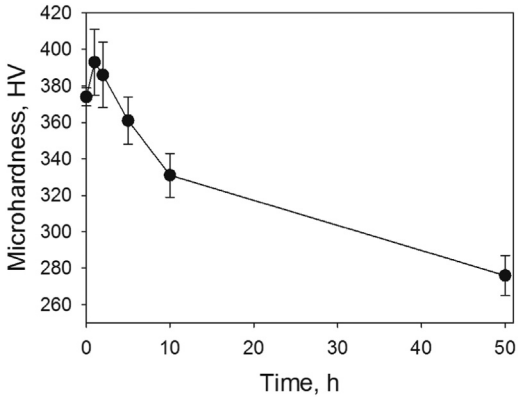

Fig. 6. Dependence of the CoCrFeMnNi alloy microhardness on annealing time at 600 °C.

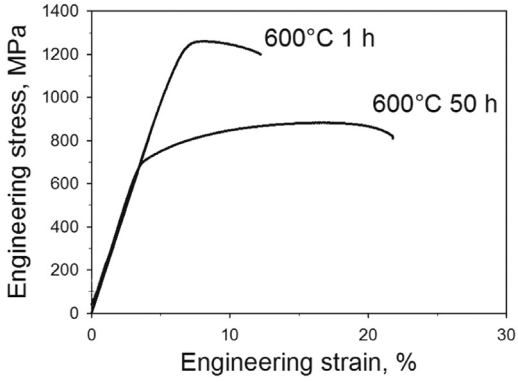

Fig. 7. Tensile stress-strain curve of the CoCrFeMnNi alloy on the annealing time at 600 °C for 1 and 50 h.

initial stages of annealing at 600 °C due to the fcc solid solution decomposition. During further annealing the bcc phase was gradually replaced with the equilibrium sigma phase.

The changes in the fractions of the constitutive phases were accompanied by grains/particles coarsening (Table 3, Fig. 4). Coarsening can be controlled by volume diffusion if the growth exponents n = 3 [39], or by diffusion along grain boundaries if n = 4 [40]. In the present case, the sigma particles coarsening seems to be controlled mainly by grain boundary diffusion with n = 4 (Fig. 4) taking into account their preferable location at grain boundaries. Meanwhile the bcc particles exhibited much slower coarsening kinetics with n = 7, that can be associated with the phase dissolution during annealing due to the non-equilibrium nature. The fcc grains coarsening kinetics (n = 3.6) only slightly faster than that of the grain boundary sigma particles thereby suggesting the main contribution of grain boundary diffusion to fcc grains growth. It should be noted that the found fcc grain growth exponent is higher than that reported for annealing in the single-phase region at 850–950 °C (n = 3) [27].

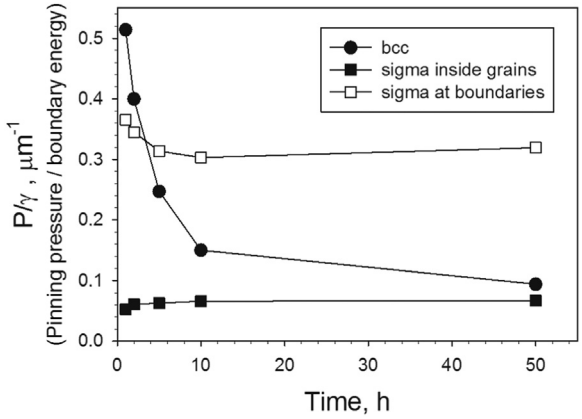

Fig. 8. Grain boundary energy normalized pinning pressures from different particles in the CoCrFeMnNi alloy during annealing at 600 °C as a function of annealing time.

Usually the coarsening kinetics in two-phase compositions with the pinning effect of the second phase particles can be described by the well-known Zener drag mechanism. Following Zener's original consideration, [41] the pinning pressure P_z on a boundary caused by homogeneously distributed spherical particles can be derived as:

$$P_Z = 3\gamma\frac{F_v}{d}, \quad (1)$$

where γ is the boundary surface energy per unit area, and Fv and d are the fraction and size of dispersed particles, respectively. When the particles are located at the boundaries, the pinning pressure P_B on a boundary depends on the ratio of particles and grains size [42] and can be evaluated as:

$$P_B = \gamma\frac{Fv_b D}{d^2}, \quad (2)$$

where D is the grain size, Fv_b is the fraction of particles at grain boundaries.

The pinning pressure on grain boundaries caused by different kinds of precipitates after different annealing times was calculated (Fig. 8) using the input parameters for the bcc particles from Table 3 and for sigma particles from Table 5. Since the sigma phase particles were found both inside grains and at grain boundaries, the pinning pressures for these cases were calculated separately using either Eq. (1) for the homogeneously distributed sigma particles or Eq. (2) for the grain boundary particles, respectively. The bcc particles pinning effect was also calculated using Eq. (1).

At relatively small annealing times (1–2 h), the maximal pinning pressure was provided by randomly distributed bcc particles due to their small size (Table 3). With increasing time the bcc precipitates induced P_z reduced rapidly, almost reaching the values for the intragranular sigma precipitates which exhibited the smallest effect for all annealing times. In contrast, the pinning pressures P_B attributed to the grain boundary sigma particles only slightly decreased with increasing the annealing time. Starting from 5 h annealing, the sigma precipitates provided the highest pinning pressures P_B (Fig. 8) obviously restricting grain growth during annealing.

The Zener limiting grain size can be calculated using the following equation [43]:

$$D_Z = \alpha\frac{2d}{3F_v} \quad (3)$$

where α is a scaling factor, d and F_v are respectively size and fraction of particles. The relationship between the experimental fcc grain size (Table 2) and the average size / average fraction of all the particles (d/F_v) ratio is plotted in Fig. 9.

Fig. 9 shows that the fcc grain size is proportional to the d/F_v ratio of

Table 5
Sigma phase particles parameters of the CoCrFeMnNi alloy after annealing at 600 °C for 1–50 h.

Annealing time, hours		1	2	5	10	50
Sigma particles inside grains	Fraction, %	0.14 ± 0.04	0.18 ± 0.05	0.23 ± 0.08	0.27 ± 0.09	0.35 ± 0.11
	Size, nm	76 ± 16	91 ± 18	110 ± 13	123 ± 11	157 ± 20
Sigma particles at grain boundaries	Fraction, %	1.9 ± 0.7	2.4 ± 0.8	3.7 ± 1.4	5.1 ± 2.1	7.0 ± 2.2
	Size, nm	260 ± 47	305 ± 30	493 ± 36	584 ± 25	817 ± 57

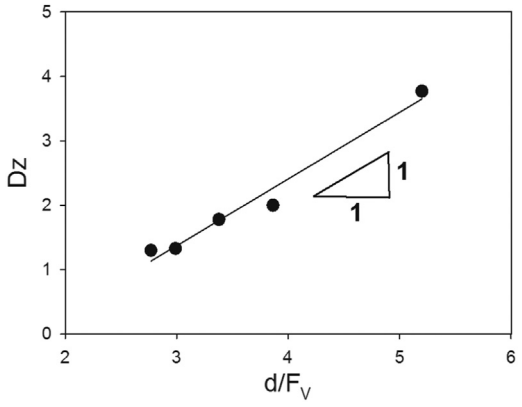

Fig. 9. Dependence of fcc grain size (D_Z) on size / fraction of the particles (d/F_v) ratio.

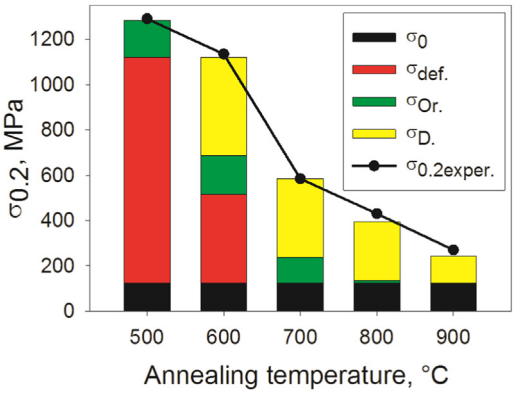

Fig. 10. Contributions of different strengthening mechanisms in the CoCrFeMnNi alloy depending on isochronal (1 h) annealing temperature.

the particles with α = 1.5 which is larger than those commonly accepted, however. Usually the value of α = 1.0, however some authors use 0.25 < α < 0.5 [44,45]. The obtained increased value of α can be associated with the particles instabilities during grain growth [43]. Nevertheless the linear dependence confirms that the grain growth of the fcc grains was controlled by the Zener pinning effect of the particles due to which the fcc grains remained relatively small (3.8 μm) even after 50 h annealing at 600 °C.

4.2. Strengthening mechanisms

The obtained data on mechanical properties of the annealed alloy expectably shows that strength/hardness of the alloy became lower with an increase in the annealing temperature or time while ductility increased (Figs. 5–7) as a result of recrystallization of the cold-worked microstructure (Figs. 1 and 2). However, some increment in strength/hardness after a short (1–2 h) annealing at low temperatures (500–600 °C) seems to be quite unusual. To get better understanding of the microstructure-mechanical properties relationship in the alloy we have performed qualitative analysis of the strengthening mechanisms.

The contribution of different strengthening mechanisms into the overall strength of the alloy can be determined as:

$$\sigma = \sigma_0 + \sigma_{def.} + \sigma_{D.} + \sigma_{Or.}, \quad (4)$$

where σ_0 is the Pieirls stress, $\sigma_{def.}$ is the work (cold rolling) strengthening:

$$\sigma_{def.} = \sigma_{0.2}(80\%rolling)*(1-V_{rec.}) \quad (5)$$

$\sigma_{D.}$ is the grain boundary (Hall-Petch) strengthening:

$$\sigma_{D.} = K_y * D^{-1/2} \quad (6)$$

$\sigma_{Or.}$ is the precipitation (Orowan) strengthening [46]:

$$\sigma_{Or.} = \left(\frac{0.538Gbf^{\frac{1}{2}}}{d}\right) ln\left(\frac{d}{2b}\right) \quad (7)$$

Here $\sigma_{0.2}$ *(80% rolling)* is the yield strength of the cold-rolled alloy, V_{rec} and D are the volume fraction and size of recrystallized fcc grains, respectively, K_y – the Hall-Petch coefficient, G – the shear modulus, b is the Burgers vector, f and d denote, respectively, the fraction and size of the precipitates. The values of σ_0 = 125 MPa, K_y = 494 MPa/μm$^{-1/2}$, G = 80 GPa, and $b = 2.58 \times 10^{-10}$ m were adopted from [10,31], while $\sigma_{0.2}$, V_{rec}, D, f, and d were determined experimentally (Tables 1 and 4). The obtained results for the isochronal annealing for 1 h at 500–900 °C are shown in Fig. 10.

Fig. 10 shows good agreement between the calculated and the experimental values of the yield strength of the CoCrFeMnNi alloy after annealed at different temperatures. After annealing at 500–600 °C work hardening ($\sigma_{def.}$) contributes greatly to the overall strength, but the increase in the yield strength in comparison to the cold rolled condition can be attributed to the bcc and sigma phases precipitation ($\sigma_{Or.}$). Work hardening strengthening diminishes at temperatures of 700 °C and above due to the formation of a completely recrystallized microstructure (Fig. 2). Also, both precipitation hardening and grain boundary strengthening started to decrease continuously with an increase in the annealing temperature above 700 °C due to particles/grains coarsening (Table 1). For the precipitation hardening, the decrease in the particles fraction (Table 1) also had a negative effect on strengthening. Overall the graph showed that the highest strength increment after annealing at 700 °C and 800 °C was provided by the grain boundaries ($\sigma_{D.}$). Only in the coarse grain microstructure, which was formed during annealing at 900 °C, grain size strengthening was approximately equal to σ_0.

In the case of the isothermal annealing at 600 °C softening (Figs. 6–7) is likely to be governed by the same processes: recrystallization and fcc phase grain growth. Coarsening of the sigma phase particles was accompanied by a pronounced increase in their fraction thereby diminishing the σ_{Or} effect on strength. Indeed, the calculated values of $\sigma_{Or.}$ are 170 MPa and 156 MPa after annealing for 1 and 50 h at 600 °C, respectively. After 50 h annealing the greatest contribution was provided by grain boundary strengthening (300 MPa) due to fine (3.7 μm) fcc grains (Table 3). The calculated strength (sum of the all strengthening mechanisms contribution) is reasonably close to the experimental value – 580 MPa and 685 MPa, respectively.

The attractive combination of strength and ductility of the CoCrFeMnNi alloy after annealing at 600 °C for 50 h (Fig. 6) can therefore be mainly attributed to the fine-grained fully recrystallized fcc matrix [47]. However one must keep in mind that the second (mostly,

sigma) phase particles are responsible for the preserving fine size of fcc grains (Fig. 9) thereby *indirectly* contributing to high mechanical properties of the alloy. Similar behavior has been recently reported for several other HEAs [24,48].

In summary, the results obtained in the current study have demonstrated that second phase precipitates can have a pronounced effect on the mechanical properties of the CoCrFeMnNi high entropy alloy, widely considered as a single phase alloy. This effect can be direct (via precipitation hardening) or indirect (via pinning of the fcc matrix grain boundaries). The current development strategy of the high-strength HEAs is strongly associated with the finding of a single-phase composition which would be prone to the formation of strengthening second phases due to alloying with additional elements [14]. The results of the present work suggest that HEAs with a single-phase structure stable at high temperatures can be strengthened not only by the alloying but also by a proper thermomechanical/thermal treatment resulting in the formation of precipitates that either directly impede dislocation motion [19,20] or strongly restrict grain growth [24] (Figs. 9–10). It should be noted that recent results show the applicability of such approach not only for the 3d transition metals HEAs with an fcc structure, but also for refractory HEAs with a bcc structure like HfNbTaTiZr alloy [30,49].

5. Conclusions

In this work, structure and mechanical properties of the CoCrFeMnNi high entropy alloy after cold rolling and subsequent annealing at 500–900 °C for 1–50 h were examined. Following conclusions were drawn:

1) Isochronal annealing at 500–900 °C for 1 h resulted in recrystallization of the fcc matrix (600–900 °C) and precipitation of the Cr-rich bcc (500–700 °C) and sigma (600–800 °C) particles. The size and fraction of the recrystallized fcc grains and size of the bcc/sigma particles increased with the annealing temperature. The fraction of the second phase particles exhibited a non-monotonic dependence on the annealing temperature.
2) Isothermal annealing at 600 °C resulted in the growth of the recrystallized fcc grains and coarsening of both the sigma and bcc particles. Grain growth and sigma particle coarsening can be expressed by power law functions of annealing time with the grain/particle size exponents of about 3.6 and 4, respectively. Furthermore, it was found that the fcc grain growth was limited by the particles as per the Zener drag mechanism. An increase in the annealing time at 600 °C from 1–50 h was also accompanied by a pronounced increase in the fraction of the sigma phase and a decrease in the fraction of the bcc phase.
3) Strength of the alloy increased after annealing for 1 h at 500 °C and 600 °C in comparison with the cold rolled condition, while annealing at higher temperatures resulted in pronounced softening together with increased ductility. The quantitative analysis had revealed that strengthening after annealing at low temperatures was associated with the bcc/sigma particles precipitation.
4) Increase of the annealing time at 600 °C from 1 h to 50 h resulted in softening and increase of ductility. However, even after 50 h annealing the alloy maintained relatively high strength (yield strength of 685 MPa) which can be ascribed to the grain boundary (Hall-Petch) strengthening due to fine fcc grains preserved by pinning effect of the sigma particles.

Acknowledgments

The authors gratefully acknowledge the financial support from the Russian Science Foundation Grant no. 18-19-00003. The authors are grateful to the personnel of the Joint Research Center, “Technology and Materials”, Belgorod State University, for their assistance.

References

[1] D.B. Miracle, O.N. Senkov, A critical review of high entropy alloys and related concepts, Acta Mater. 122 (2017) 448–511, https://doi.org/10.1016/j.actamat.2016.08.081.
[2] B. Cantor, I.T.H. Chang, P. Knight, A.J.B. Vincent, Microstructural development in equiatomic multicomponent alloys, Mater. Sci. Eng. A. 375 (2004) 213–218, https://doi.org/10.1016/j.msea.2003.10.257.
[3] F. Otto, Y. Yang, H. Bei, E.P.P. George, Relative effects of enthalpy and entropy on the phase stability of equiatomic high-entropy alloys, Acta Mater. 61 (2013) 2628–2638, https://doi.org/10.1016/j.actamat.2013.01.042.
[4] F. Otto, A. Dlouhý, K.G. Pradeep, M. Kuběnová, D. Raabe, G. Eggeler, E.P. George, Decomposition of the single-phase high-entropy alloy CrMnFeCoNi after prolonged anneals at intermediate temperatures, Acta Mater. 112 (2016), https://doi.org/10.1016/j.actamat.2016.04.005.
[5] E.J. Pickering, R. Muñoz-Moreno, H.J. Stone, N.G. Jones, Precipitation in the equiatomic high-entropy alloy CrMnFeCoNi, Scr. Mater. 113 (2016), https://doi.org/10.1016/j.scriptamat.2015.10.025.
[6] B. Schuh, F. Mendez-Martin, B. Völker, E.P. George, H. Clemens, R. Pippan, A. Hohenwarter, Mechanical properties, microstructure and thermal stability of a nanocrystalline CoCrFeMnNi high-entropy alloy after severe plastic deformation, Acta Mater. 96 (2015) 258–268, https://doi.org/10.1016/j.actamat.2015.06.025.
[7] N.D. Stepanov, D.G. Shaysultanov, M.S. Ozerov, S.V. Zherebtsov, G.A. Salishchev, Second phase formation in the CoCrFeNiMn high entropy alloy after recrystallization annealing, Mater. Lett. 185 (2016) 1–4, https://doi.org/10.1016/j.matlet.2016.08.088.
[8] W. Zhou, L.M. Fu, P. Liu, X.D. Xu, B. Chen, G.Z. Zhu, X.D. Wang, A.D. Shan, M.W. Chen, Deformation stimulated precipitation of a single-phase CoCrFeMnNi high entropy alloy, Intermetallics 85 (2017) 90–97, https://doi.org/10.1016/j.intermet.2017.02.010.
[9] A. Gali, E.P. George, Tensile properties of high- and medium-entropy alloys, Intermetallics 39 (2013) 74–78, https://doi.org/10.1016/j.intermet.2013.03.018.
[10] F. Otto, A. Dlouhý, C. Somsen, H. Bei, G. Eggeler, E.P. George, The influences of temperature and microstructure on the tensile properties of a CoCrFeMnNi high-entropy alloy, Acta Mater. 61 (2013) 5743–5755, https://doi.org/10.1016/j.actamat.2013.06.018.
[11] B. Gludovatz, A. Hohenwarter, D. Catoor, E.H. Chang, E.P. George, R.O. Ritchie, A fracture-resistant high-entropy alloy for cryogenic applications, Science 345 (2014) 1153–1158, https://doi.org/10.1126/science.1254581.
[12] J.Y. He, H. Wang, H.L. Huang, X.D. Xu, M.W. Chen, Y. Wu, X.J. Liu, T.G. Nieh, K. An, Z.P. Lu, A precipitation-hardened high-entropy alloy with outstanding tensile properties, Acta Mater. 102 (2016) 187–196, https://doi.org/10.1016/j.actamat.2015.08.076.
[13] Y.Y. Zhao, H.W. Chen, Z.P. Lu, T.G. Nieh, Thermal stability and coarsening of coherent particles in a precipitation-hardened (NiCoFeCr)94Ti2Al4 high-entropy alloy, Acta Mater. 147 (2018) 184–194, https://doi.org/10.1016/J.ACTAMAT.2018.01.049.
[14] W.H. Liu, T. Yang, C.T. Liu, Precipitation hardening in CoCrFeNi-based high entropy alloys, Mater. Chem. Phys. (2017), https://doi.org/10.1016/j.matchemphys.2017.07.037.
[15] N.D. Stepanov, N.Y. Yurchenko, M.A. Tikhonovsky, G.A. Salishchev, Effect of carbon content and annealing on structure and hardness of the CoCrFeNiMn-based high entropy alloys, J. Alloy. Compd. 687 (2016) 59–71, https://doi.org/10.1016/j.jallcom.2016.06.103.
[16] N. Kashaev, V. Ventzke, N. Stepanov, D. Shaysultanov, V. Sanin, S. Zherebtsov, Laser beam welding of a CoCrFeNiMn-type high entropy alloy produced by self-propagating high-temperature synthesis, Intermetallics 96 (2018) 63–71, https://doi.org/10.1016/j.intermet.2018.02.014.
[17] B. Gwalani, V. Soni, M. Lee, S. Mantri, Y. Ren, R. Banerjee, Optimizing the coupled effects of Hall-Petch and precipitation strengthening in a Al0.3CoCrFeNi high entropy alloy, Mater. Des. 121 (2017) 254–260, https://doi.org/10.1016/j.matdes.2017.02.072.
[18] B. Gwalani, S. Gorsse, D. Choudhuri, M. Styles, Y. Zheng, R.S. Mishra, R. Banerjee, Modifying transformation pathways in high entropy alloys or complex concentrated alloys via thermo-mechanical processing, Acta Mater. 153 (2018) 169–185, https://doi.org/10.1016/J.ACTAMAT.2018.05.009.
[19] K. Ming, X. Bi, J. Wang, Realizing strength-ductility combination of coarse-grained Al0.2Co1.5CrFeNi1.5Ti0.3alloy via nano-sized, coherent precipitates, Int. J. Plast. 100 (2018) 177–191, https://doi.org/10.1016/j.ijplas.2017.10.005.
[20] M.V. Klimova, D.G. Shaysultanov, R.S. Chernichenko, V.N. Sanin, N.D. Stepanov, S.V. Zherebtsov, A.N. Belyakov, Recrystallized microstructures and mechanical properties of a C-containing CoCrFeNiMn-type high-entropy alloy, Mater. Sci. Eng. A. 740–741 (2019) 201–210, https://doi.org/10.1016/J.MSEA.2018.09.113.
[21] N.D. Stepanov, D.G. Shaysultanov, G.A. Salishchev, M.A. Tikhonovsky, E.E. Oleynik, A.S. Tortika, O.N. Senkov, Effect of V content on microstructure and mechanical properties of the CoCrFeMnNiVx high entropy alloys, J. Alloy. Compd. 628 (2015) 170–185, https://doi.org/10.1016/j.jallcom.2014.12.157.
[22] Y.H. Jo, W.-M. Choi, S.S. Sohn, H.S. Kim, B.-J. Lee, S. Lee, Role of brittle sigma phase in cryogenic-temperature-strength improvement of non-equi-atomic Fe-rich VCrMnFeCoNi high entropy alloys, Mater. Sci. Eng. A. 724 (2018) 403–410, https://doi.org/10.1016/J.MSEA.2018.03.115.
[23] J.W. Bae, J. Moon, M.J. Jang, D. Yim, D. Kim, S. Lee, H.S. Kim, Trade-off between tensile property and formability by partial recrystallization of CrMnFeCoNi high-entropy alloy, Mater. Sci. Eng. A. 703 (2017) 324–330, https://doi.org/10.1016/J.MSEA.2017.07.079.

[24] N.D. Stepanov, D.G. Shaysultanov, R.S. Chernichenko, D.M. Ikornikov, V.N. Sanin, S.V. Zherebtsov, Mechanical properties of a new high entropy alloy with a duplex ultra-fine grained structure, Mater. Sci. Eng. A. 728 (2018) 54–62, https://doi.org/10.1016/j.msea.2018.04.118.
[25] H.Y. Yasuda, H. Miyamoto, K. Cho, T. Nagase, Formation of ultrafine-grained microstructure in Al0.3CoCrFeNi high entropy alloys with grain boundary precipitates, Mater. Lett. 199 (2017) 120–123, https://doi.org/10.1016/J.MATLET.2017.04.072.
[26] K. Liu, M. Komarasamy, B. Gwalani, S. Shukla, R.S. Mishra, Fatigue behavior of ultrafine grained triplex Al0.3CoCrFeNi high entropy alloy, Scr. Mater. 158 (2019) 116–120, https://doi.org/10.1016/J.SCRIPTAMAT.2018.08.048.
[27] W.H. Liu, Y. Wu, J.Y. He, T.G. Nieh, Z.P. Lu, Grain growth and the Hall-Petch relationship in a high-entropy FeCrNiCoMn alloy, Scr. Mater. 68 (2013) 526–529, https://doi.org/10.1016/j.scriptamat.2012.12.002.
[28] F. Otto, N.L. Hanold, E.P. George, Microstructural evolution after thermomechanical processing in an equiatomic, single-phase CoCrFeMnNi high-entropy alloy with special focus on twin boundaries, Intermetallics 54 (2014) 39–48, https://doi.org/10.1016/j.intermet.2014.05.014.
[29] Z. Wu, H. Bei, F. Otto, G.M. Pharr, E.P. George, Recovery, recrystallization, grain growth and phase stability of a family of FCC-structured multi-component equiatomic solid solution alloys, Intermetallics 46 (2014), https://doi.org/10.1016/j.intermet.2013.10.024.
[30] O.N. Senkov, A.L. Pilchak, S.L. Semiatin, Effect of cold deformation and annealing on the microstructure and tensile properties of a HfNbTaTiZr refractory high entropy alloy, Metall. Mater. Trans. A. (2018) 1–17, https://doi.org/10.1007/s11661-018-4646-8.
[31] N. Stepanov, M. Tikhonovsky, N. Yurchenko, D. Zyabkin, M. Klimova, S. Zherebtsov, A. Efimov, G. Salishchev, Effect of cryo-deformation on structure and properties of CoCrFeNiMn high-entropy alloy, Intermetallics 59 (2015) 8–17, https://doi.org/10.1016/j.intermet.2014.12.004.
[32] P.A. Beck, J.C. Kremer, L. Demer, Grain growth in high purity aluminum, Phys. Rev. 71 (1947), https://doi.org/10.1103/PhysRev.71.555 (555–555).
[33] P.P. Bhattacharjee, G.D. Sathiaraj, M. Zaid, J.R. Gatti, C. Lee, C.W. Tsai, J.W. Yeh, Microstructure and texture evolution during annealing of equiatomic CoCrFeMnNi high-entropy alloy, J. Alloy. Compd. 587 (2014) 544–552, https://doi.org/10.1016/j.jallcom.2013.10.237.
[34] G.D. Sathiaraj, M.Z. Ahmed, P.P. Bhattacharjee, Microstructure and texture of heavily cold-rolled and annealed fcc equiatomic medium to high entropy alloys, J. Alloy. Compd. 664 (2016) 109–119, https://doi.org/10.1016/j.jallcom.2015.12.172.
[35] J.E. Saal, I.S. Berglund, J.T. Sebastian, P.K. Liaw, G.B. Olson, Equilibrium high entropy alloy phase stability from experiments and thermodynamic modeling, Scr. Mater. 146 (2018) 5–8, https://doi.org/10.1016/J.SCRIPTAMAT.2017.10.027.
[36] N.D. Stepanov, D.G. Shaysultanov, R.S. Chernichenko, M.A. Tikhonovsky, S.V. Zherebtsov, Effect of Al on structure and mechanical properties of Fe-Mn-Cr-Ni-Al non-equiatomic high entropy alloys with high Fe content, J. Alloy. Compd. 770 (2018) 194–203, https://doi.org/10.1016/j.jallcom.2018.08.093.
[37] C.-C. Hsieh, W. Wu, Overview of intermetallic sigma ( ) phase precipitation in stainless steels, ISRN Metall. 2012 (2012) 1–16, https://doi.org/10.5402/2012/732471.
[38] E.O. Hall, S.H. Algie, The sigma phase, Metall. Rev. 11 (1966) 61–88, https://doi.org/10.1179/mtlr.1966.11.1.61.
[39] M. Hillert, On the theory of normal and abnormal grain growth, Acta Metall. 13 (1965) 227–238, https://doi.org/10.1016/0001-6160(65)90200-2.
[40] A. Ardell, On the coarsening of grain boundary precipitates, Acta Metall. 20 (1972) 601–609, https://doi.org/10.1016/0001-6160(72)90015-6.
[41] G.S. Rohrer, Introduction to grains, phases, and interfaces—an interpretation of microstructure (by C.S. Smith, Metall. Mater. Trans. A. 41 (2010) 1063–1100), Trans. AIME 175 (1948) 15–51, https://doi.org/10.1007/s11661-010-0215-5.
[42] W.B. Hutchinson, B.J. Duggan, Influence of precipitation on recrystallization and texture development in an iron-1.2% copper alloy, Met. Sci. 12 (1978) 372–380, https://doi.org/10.1179/msc.1978.12.8.372.
[43] F.J. Humphreys, M. Hatherly, Recrystallization and Related Annealing Phenomena, Elsevier, 2004.
[44] N. Louat, The resistance to normal grain growth from a dispersion of spherical particles, Acta Metall. 30 (1982) 1291–1294, https://doi.org/10.1016/0001-6160(82)90147-X.
[45] M. Hillert, Inhibition of grain growth by second-phase particles, Acta Metall. 36 (1988) 3177–3181, https://doi.org/10.1016/0001-6160(88)90053-3.
[46] T. Gladman, Precipitation hardening in metals, Mater. Sci. Technol. 15 (1999) 30–36, https://doi.org/10.1179/026708399773002782.
[47] S.J. Sun, Y.Z. Tian, H.R. Lin, X.G. Dong, Y.H. Wang, Z.J. Zhang, Z.F. Zhang, Enhanced strength and ductility of bulk CoCrFeMnNi high entropy alloy having fully recrystallized ultrafine-grained structure, Mater. Des. 133 (2017) 122–127, https://doi.org/10.1016/j.matdes.2017.07.054.
[48] Z. Wang, A. Genc, I. Baker, Direct versus indirect particle strengthening in a strong, ductile FeNiMnAlTi high entropy alloy, Mater. Charact. 132 (2017) 156–161, https://doi.org/10.1016/J.MATCHAR.2017.08.019.
[49] N.D. Stepanov, N.Y. Yurchenko, S.V. Zherebtsov, M.A. Tikhonovsky, G.A. Salishchev, Aging behavior of the HfNbTaTiZr high entropy alloy, Mater. Lett. 211 (2018) 87–90, https://doi.org/10.1016/j.matlet.2017.09.094.